Chalcogenide Letters Vol. 16, No. 12, December 2019, p. 615 - 629

SILVER-CADMIUM CHALCOGENIDE/POLYAMIDE COMPOSITE MATERIALS INVESTIGATED FROM MORPHOLOGICAL AND OPTICAL VIEWPOINT

N. DUKŠTIENĖ*, V. KRYLOVA
Department of Physical and Inorganic Chemistry, Kaunas University of Technology, Radvilenu st. 19, LT-50254, Kaunas, Lithuania

In present study, morphological and optical properties of silver-cadmium chalcogenide/polyamide composites were investigated. These composites were synthesised via cation-cation exchange reaction using organic−inorganic hybrid cadmium chalcogenide/polyamide composite as a starting material. Obtained composites were characterized by optical microscopy, scanning electron microscopy and ultraviolet-visible spectroscopy techniques. After the Cd^{2+} replacement with Ag^{+}, the surface morphology of the starting material transfers to a complex architecture. Optical parameters such as optical band gap, Urbach energy and steepness parameter were determined from UV-Vis spectra. The refractive index and dielectric constant of each sample were calculated at the fundamental absorption edge via various empirical relations.

(Received August 22, 2019; Accepted December 11, 2019)

Keywords: Metal chalcogenides, Organic-inorganic hybrid composites, Morphology, Optical properties

1. Introduction

Research on hybrid organic−inorganic materials (HOIMs) synthesis through combining various organic polymers and inorganic I/II–VI group semiconductor materials has been tremendously growing scientific area during the last 20 years. The properties of these HOIMs combine the best properties of both organic polymer and inorganic semiconductrors constituents and can be tuanable over a broad range. The unusual properties of organic polymers − inorganic I/II–VI group semiconductor hybrids make them sutable for electro-optical applications such as soral cells [1–2], EDL capacitors and pseudo capacitors [3–4].

A variety of these versatile functional composites can be assessed through different fabrication routes including spin coating [5], plasma enhanced chemical vapor deposition [6], chemical modification of inorganic nanostructures surfaces [7–8], layer by layer spin coating [9], chemical bath deposition [10–12] and etc.

Despite the numerous of developed mehods, a simple and low-cost synthesis route still represents a great chalange. Cation-cation exchange reactions from pre-synthesized nanostructures have been increasingly applied as an extremely simple and economic way for accessing novel nanomaterials [13–17]. Recently, our group has applied cation-cation exchange reaction strategy to HOIMs synthesis [18]. To the best of author knowlage it has been the first publication for silver-cadmium chalcogenide/polyamide composites synthesis via cation-cation exchange reaction method. The cadmium chalcogenide/polyamide hybrid material was used as a starting material for partial conversion to silver-cadmium chalcogenide/polyamide composite. XRD patterns showed a complex composition with polycrystalline CdSe, Ag_2S and Ag_2Se peaks. XPS analysis indicates that the silver chalcogenides are located subsurface as opposed to the outermost layer that is likely Ag_2O [18]. It is worth nothing that properties of these silver-cadmium chalcogenide/polyamide composites are unknown and requires extensive studies. Low-cost polyamide 6 pocesses procesabillity and has excellent mechanical, thermal and tribological properties. The hexsagonal cadmium selenide is an *n*-type semiconductor material with a moderate bulk band gap at 300˚K of

*Corresponding author. nijole.dukstiene@ktu.lt

1.74 eV [19], which is independent of synthesis method. Both silver selenide and silver sulphide are the *n*-type semiconductors with a direct narrow band gap at at room temperature of 1.2 eV and about 1 eV, respectivly [20–21]. The multi step modifying of wide gap polyamide 6 ($E_{op.g}$ = 3.75 eV [23]) semiconductor via the introduction of silver-cadmium chalcogenides in the polymer host forms an uniform sequential arrangement of layers with different chemical and structural composition and creates the presence of various interfacial interactions, which in turn plays a strong role in optical, electrical, mechanical, thermal and other properties. Covalent, hydrogen and electroststic bonds formed between polyamide 6 functional groups and inorganic constituents [22–23] also create a large number of additional light absorption centers. The combination of both wide band polyamide 6 and narrow band semiconductors (Ag_2S and Ag_2Se) as well as a large number of additional light absorption centers in chalcogenizided polyamide 6 host [22–24] shoud also result in hight excitation coefficient, broad spectral responce to light absorption and efficient energy transfer. In this context, the multi pase silver-cadmium chalcogenides/polyamide composite could therefore be considered as potential material for optoelectronic applications. The optical constants of these compex composites such as optical band gap, refractive index, dielectric constants and other are very essential for future optical devices.

The present paper is a continuation of our recent reaserch and aims to characterize the silver-cadmium chalcogenide/polyamide composites, in particular, regarding their morphological and optical properties. A complex comparative analysis was performed by using optical microscopy, scanning electron microscopy and UV-Vis analyses. The results discussed in this paper give a better understanding of the relationship between composite morphology and optical properties and are expected to provide important insights for future engineering of silver-cadmium chalcogenide/polyamide composites.

2. Experimental details

2.1 Silver-cadmium chalcogenide/polyamide composite synthesis

The starting cadmium chalcogenide/polyamide composites and silver-cadmium chalcogenide/polyamide composites were synthesised according to the procedure described in our recent publications [18, 22–23, 25]. The synthesis steps and sample labelling are presented in Table 1.

Table 1. Experimental conditions of silver-cadmium chalcogenide/polyamide composite synthesis and sample labelling.

First step	Second step	Third step
PA 6 exposure time (min) in acidified 0.05 M $K_2SeS_2O_6$ at 60^{o}C	Chalcogen/polyamide composite in 0.1 M $Cd(CH_3COO)_2$ for 10 min at 60^{o}C	Cadmium chalcogenide/polyamide composite in 0.1 M $AgNO_3$ for 10 min at 20^{o}C
60	S1	O1
180	S2	O2
240	S3	O3

The displacement of Cd^{2+} ions from these pre-synthesized cadmium chalcogenide/polyamide composites proceeded via cation-cation exchange reaction. The schematic structures of obtained silver-cadmium chalcogenide/polyamide composites are shown in Scheme 1.

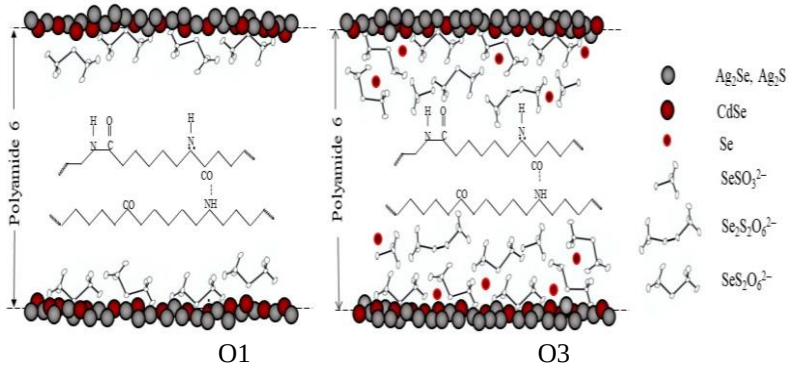

Scheme 1. The schematic structure of obtained silver-cadmium chalcogenide/polyamide composites.

2.2 Composites characterization

Optical microscopy of starting materials samples and modified by silver chalcogenides was carried out with an optical microscope Olympus CX31 (Olympus, Japan) and a photo camera Olympus C-5050 (Olympus, Japan), magnification 100×.

Scanning electron microscope images were acquired by employing a Phillips FEI XL30 FEG-ESEM and FEI Sirion HR-SEM using the accelerating voltage of 1 kV and magnification 100000×. No sample preparation (coating) before imaging was performed.

UV-Vis spectra of the composites were recorded using a Spectronic Genesys 8 UV/Visible spectrophotometer in the range between 200 and 1100 nm. Registered UV-Vis absorption spectra of the composite materials were corrected for the virgin PA 6 absorbance.

3. Results and discussion

3.1 Optical microscopy

The high activation energy for the reactant atoms and ions diffusion limits the the cation-cation exchange reaction in a bulk solid only to the top surface region [26] and a new layer in order of few nanometers is formed. In the first step an optical microscopy was applied in surface morphology analysis as it allows quicly differentiate one material from another. The optical micrographs of the starting and obtained silver-cadmium chalcogenide/polyamide materials are shown in Figure 1.

The surface morphology of the starting material is not markedly influenced by syntheses conditions. As it can be seen from Fig. 1 left column, the small spherical particles (marked as I) are densely distributed throughout the surface of all starting materials. The long narrow channels (marked as II) are also clearly observed in various areas. After cattion-cation exchge reaction, the surface morphology of silver-cadmium chalcogenide/polyamide composite becomes rougher and heterogeneous as compared with that of corresponding starting material (Fig. 1, right column). However, the obtained thin layer does not peel from the substrate suggesting material's strong mechanical adhesion with the surface.

In O1 hybrid material OM image (Fig. 1, right column), one can easily see pinholes (marked as I), individual particles (marked as II) and agglometrates (marked as III). The size of the agglomerates as well as the surface heterogeneity depends on polyamide 6 chalcogenization time. In OM images of O2 and O3 hybrid materials the different-sized particles are generally located in the large area agglomerates (marked as I) and deep well-developed channels (marked as II) are also formed on the surface.

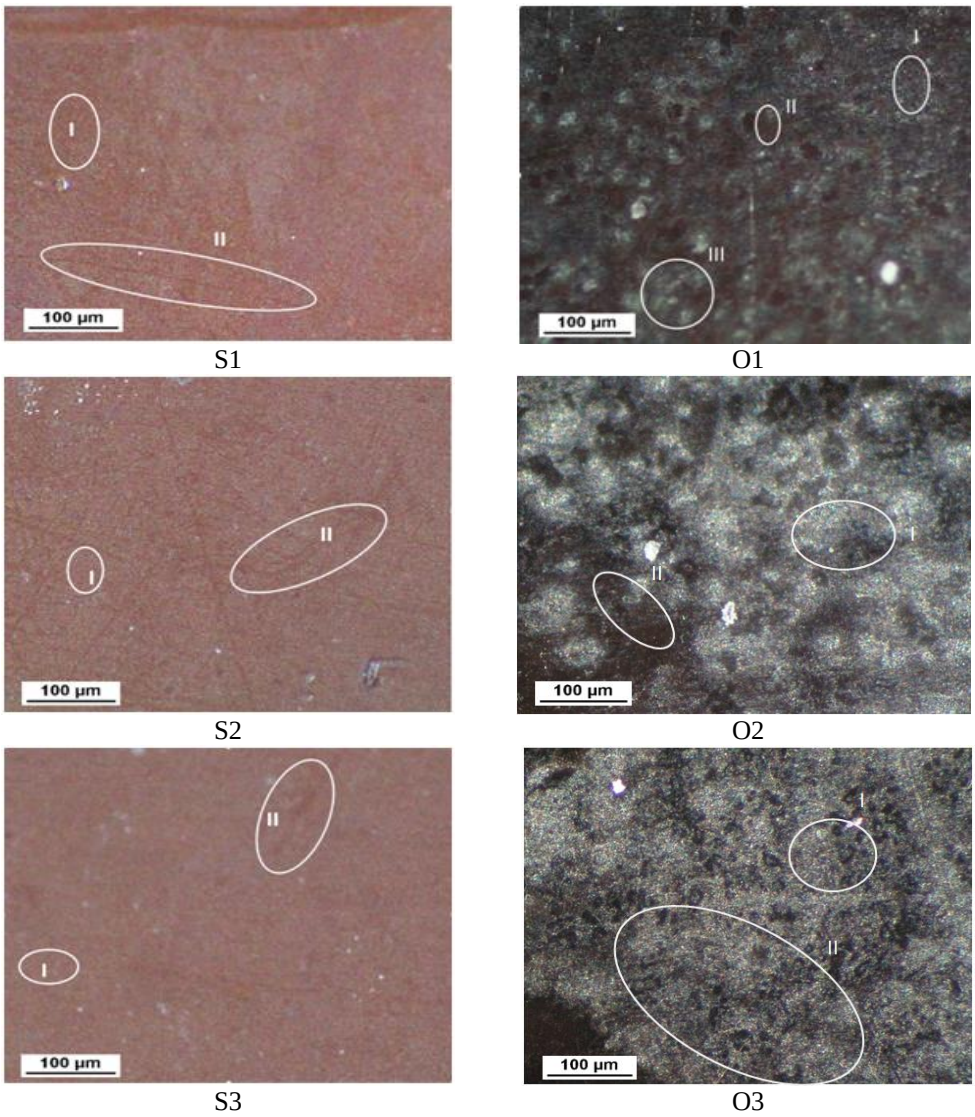

Fig. 1. Optical micrographs of starting (S) and obtained (O) silver-cadmium chalcogenide/polyamide sample. Magnification 100×.

The analysis of optical micrographs suggests that the polyamide chalcogenization time plays a decisive role in the morphology of the silver-cadmium chalcogenide/polyamide hybrid composite.

3.2 SEM analysis

Following optical microscopy the SEM analysis was performed to further characterize silver-cadmium chalcogenide/polyamide hybrid composite. The SEM images of starting and obtained silver-cadmium chalcogenide/polyamide samples are shown in Figure 2.

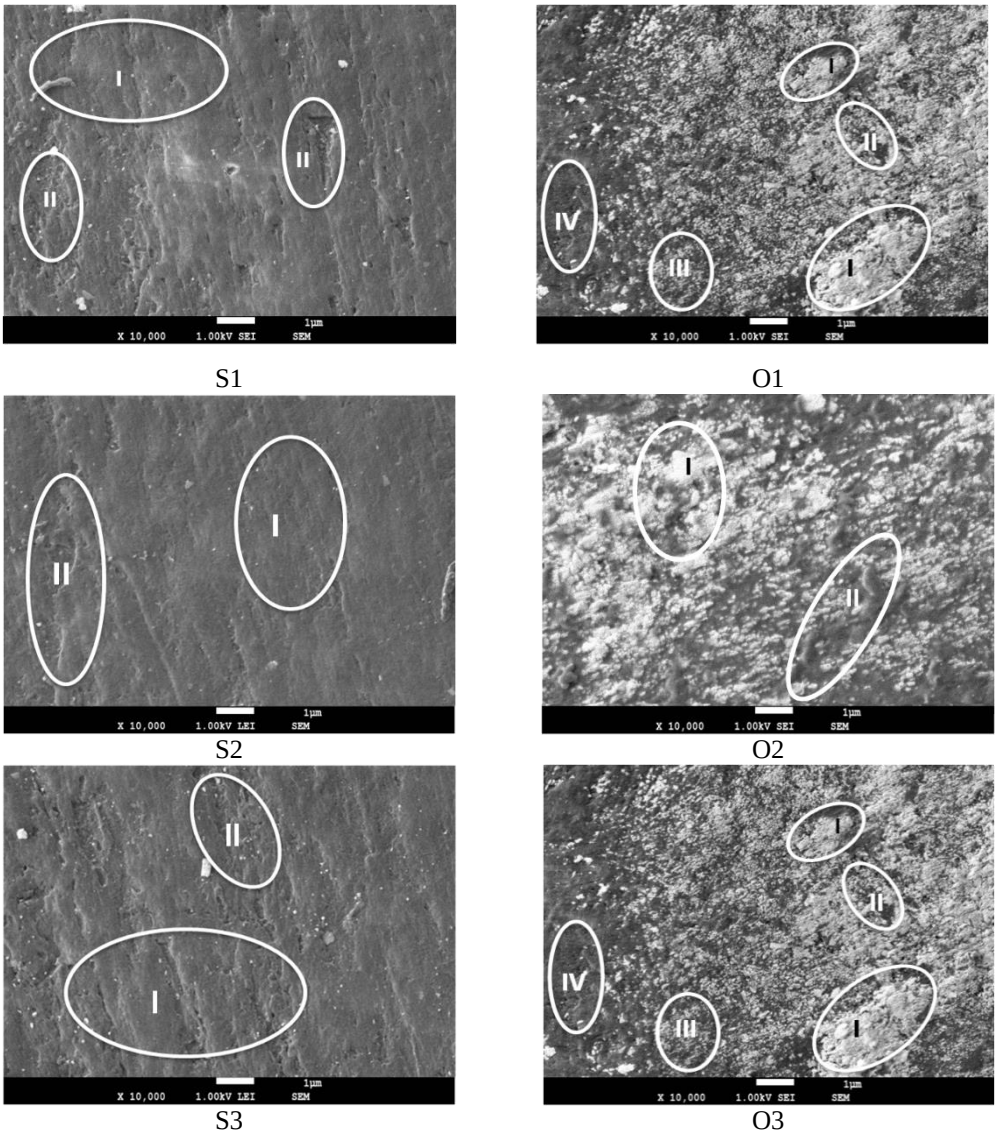

Fig. 2. SEM images of starting (S) and obtained (O) silver-cadmium chalcogenide/polyamide composite materials.

As it can be seen in the Fig. 2 left column, significant differences in the surface morphology of the different starting hybrid materials were not observed, which well coincides with the optical microscopy analysis. The SEM images show a faced surface including large-area dense and uniform blocks (marked as I) and different-sized voids (marked as II). Compared with S1 composite, the surface of O1 hybrid composite is heterogeneous and composed of different-sized agglomerates (marked as I), various voids (marked as II) and closely packed particles (marked as III). We also see some regions repeating similar morphology to that of the starting S1 material (marked as IV).

When the S2 sample was exposed to Ag^+ solution, the replacement of cadmium equalled 65.58%. In addition, the amount of selenium also decreased by 29.19% [18]. The surface morphology of O2 hybrid composite shows the number of large irregular aggregates (marked as I) and the rock-like structures (marked as II).

The replacement of Cd in the S3 starting material equals 70.56% [18]. The SEM image of O3 composite materials shows a highly inhomogeneous surface architecture composed of flat

lamellar regions (marked as I), complicated clumps (marked as II), deep voids with sharp boundaries (marked as III) and grid-like structures (marked as IV).

After the cation-cation exchange reaction, the surface morphology of the starting material transfers to a complex architecture demonstrating the influence of the cation exchanger [27].

3.3 UV-Vis analysis

3.3.1 Optical band gap energy

Absorption spectra of silver-cadmium chalcogenide/polyamide materials from 200 to 1100 nm range are presented in Figures 3, 4 and 5, respectively. For spectra interpretation, the UV-Vis spectra of starting cadmium chalcogenide/polyamide composites are also shown.

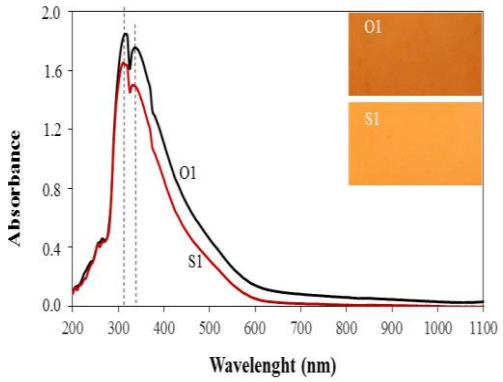

Fig. 3. UV-Vis absorption spectra and photo images of starting (S1) and obtained (O1) silver-cadmium chalcogenide/polyamide composite materials.

After cadmium chalcogenide/polyamide composites treatment in $AgNO_3$ solution, the color of the obtained samples becomes dark brown (Fig. 3, 4 and 5), suggesting the change of optical properties.

During cation-cation exchange reaction the formation of Ag_2S, CdSe, Ag_2Se as well as core-shell or heterojunction of CdSe-Ag_2S and CdSe-Ag_2Se can take place. Therefore, the formation of such complex metal chalcogenide system makes the interpretation of recorded UV-visible spectra difficult.

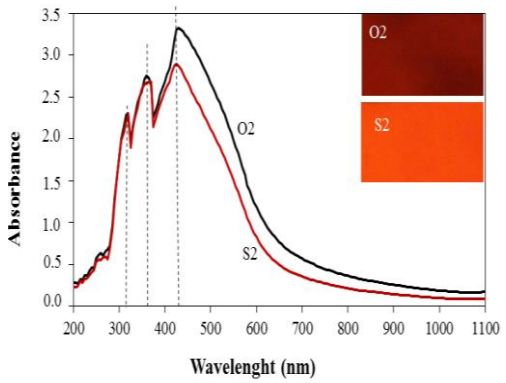

Fig. 4. UV-Vis absorption spectra and photo images of starting (S2) and obtained (O2) silver-cadmium chalcogenide/polyamide composite materials.

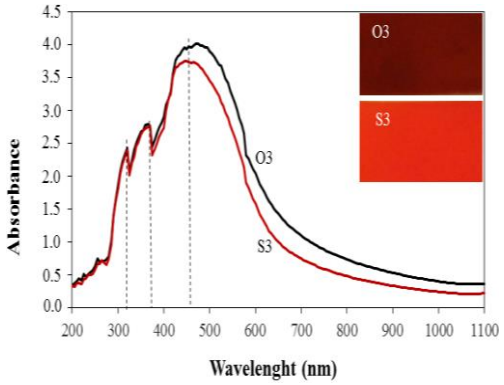

Fig. 5. UV-Vis absorption spectra and photo images of starting (S3) and obtained (O3) silver-cadmium chalcogenide/polyamide composite materials.

Chalcogenide/polyamide composite materials UV-Vis spectra display absorption peaks at 270 nm and 320 nm corresponding to absorbed $SeS_2O_6^{2-}$ ion species, and peaks at 345 and 395 nm resulting from adsorbed $SeSO_3^{2-}$ and $Se_2S_2O_6^{2-}$ ions, respectively [23]. Amorphous Se absorbs 475 nm light [28].

In the cadmium chalcogenide/polyamide composites the absorption maxima in the 300–320 nm, 335–365 nm and 400–600 nm spectral region result from combination of two different bandgap materials, both CdSe and CdS [25].

The absorption bands for nanoparticles of Ag_2S appear around 330 nm and slightly lower wavelengths of 316–320 nm [29–30]. Ag_2S nanofibers display an absorption peak at about 530 nm [31]. Ag_2Se nanoparticles absorb in the broad spectral region between 300 and 600 nm [32], while the quantum dots spectrum shows two sharp peaks at 440 and 607 nm, reaspectivly [33].

The broad absorption onsets instead of steep, sharp peaks are reported for core-shells or hetrojunctions UV-Vis absorption spectra [34–38]. CdSe-CdS core-shell quantum dots show broad absorption band in 410–545 nm spectral range [35]. The CdS-Ag_2S structures present markedly enhanced visible light absorption from 520 to 800 nm [36–38]. Doping CdSe nanocrystals with silver through cation-cation exchange reaction does not notably change CdSe UV-Vis absorption spectra [39]. Contrary, other authors stated that the formation of CdSe-Ag_2Se core shell results in complete disappearance of the CdSe absorption peak in UV-Vis spectra [40].

CdS/organic polymer composite absorbs 400–510 nm light [41–43]. The PVP/Ag_2S electrospun fibre film showed absorption at about 317 nm [44].

Based on literature survey and experimental spectra analysis three statements can be made. First, the silver-cadmium chalcogenide/polyamide composites absorption spectra are a superposition of the individual absorption spectra of different materials within polyamide 6 host. Second, the absorption edge of silver-cadmium chalcogenide/polyamide composites shifted to longer wavelengths and their absorbance increased in the 300–600 nm regions as compared with the starting materials. This red shift of absorption edge can be related with the overall complex valence band and conduction band alignment as weel as presence of numerous vacancies and defects in band gap. As discussed above, the silver-cadmium chalcogenide/polyamide composites show extremely heterogeneous surface morphology with high specific surface area, this in turn also leads to an increase of the incident light absorption. Third, the O2 and O3 composites absorb a greater portion of incident near–infrared light as compared with starting S2 and S3 composites.

Although the overlapping of absorption peaks makes their identification difficult, the tentative assignment of each absorption peak in silver-cadmium chalcogenide/polyamide composites spectra is presented in Table 2.

Table 2. Peak position and assignment of silver-cadmium chalcogenide/polyamide composites UV-Vis spectra.

Composite	Composition from XRD [18]	Peak position, nm	Peak shift as compared with starting composite, nm	Assignment	Literature
O1	hexagonal CdSe, monoclinic Ag_2S	270	0	$SeS_2O_6^{2-}$	[23]
		315	+5	$SeS_2O_6^{2-}$, Ag_2S	[23,29–30]
		340	+5	$SeSO_3^{2}$, CdSe	[23,25]
O2	hexagonal CdSe monoclinic Ag_2S orthorhombic Ag_2Se	270	0	$SeS_2O_6^{2-}$	[23]
		320	0	$SeS_2O_6^{2-}$, Ag_2S	[23,29–30]
		360	–5	$SeSO_3^{2-}$, CdSe	[23,25]
		435	+5	$Se_2S_2O_6^{2-}$, CdSe Ag_2Se	[23,25,32–33]
O3	hexagonal CdSe, monoclinic Ag_2S, orthorhombic Ag_2Se	270	0	$SeS_2O_6^{2-}$	[23]
		320	0	$SeS_2O_6^{2-}$, Ag_2S	[23,29–30]
		360	–5	$SeSO_3^{2-}$ CdSe	[23,25]
		480	+25	Se, $Se_2S_2O_6^{2-}$, CdSe, Ag_2Se	[23,25,28,32–33]

The optical band gaps ($E_{op.g}$) of the silver-cadmium chalcogenide/polyamide as well as starting materials were determined by applying absorption spectrum fitting method [45]. In absorption spectrum fitting method the fundamental absorption edge (λ_g) can be determined from the plot:

$$\left(\frac{A}{\lambda}\right)^{1/m} = f\left(\frac{1}{\lambda}\right) \tag{1}$$

where m is the index which takes values 0.5, 1.5, 2 and 3 for direct allowed, direct forbidden, indirect allowed and indirect forbidden transitions, respectively; A is the absorption; λ, is the wavelength. The extrapolating of straight line portion to cut the energy axis gives the fundamental absorption edge λ_g. Then employing the obtained value of λ_g the optical band gap $E_{op.g}$ can be directly calculated from the following relation [45–46]:

$$E_{op.g} = \frac{1239.83}{\lambda_g} \tag{2}$$

In this work the UV-Vis experimental spectra fit better the straight linear portion in the $\left(\frac{A}{\lambda}\right)^2 = f\left(\frac{1}{\lambda}\right)$ plots (Figures 6–8), which confirms the direct optical transitions of starting materials as well as obtained silver-cadmium chalcogenide/polyamide composites.

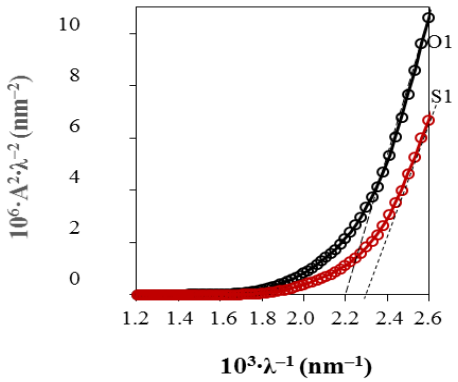

Fig. 6. Variation of $(A/\lambda)^2$ with λ^{-1} for silver-cadmium chalcogenide/polyamide O1 and starting S1 composites.

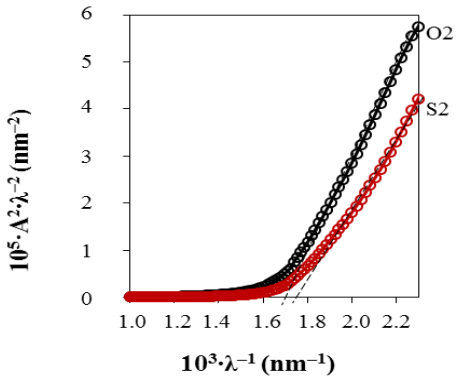

Fig. 7. Variation of $(A/\lambda)^2$ with λ^{-1} for silver-cadmium chalcogenide/polyamide O2 and starting S2 composites.

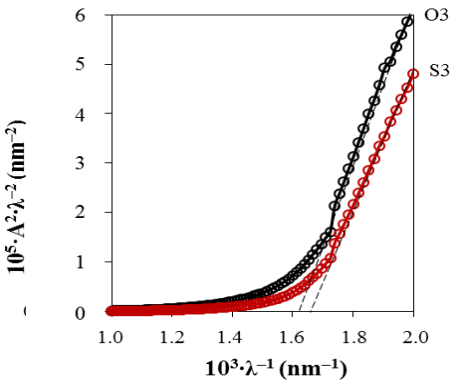

Fig. 8. Variation of $(A/\lambda)^2$ with λ^{-1} for silver-cadmium chalcogenide/polyamide O3 and starting S3 composites.

The values of optical band gap energy and the fundamental absorption edge are listed in Table 3.

Table 3. The fundamental absorption edge (λ_g), optical band gap ($E_{op.g}$), Urbach energy (E_U) and steepness parameter (σ) of studied composite materials.

Composite	λ_g, nm	$E_{op.g}$, eV	E_U, eV	σ
S1	501	2.475	0.213	0.120
O1	555	2.234	0.321	0.079
S2	592	2.094	0.307	0.084
O2	613	2.023	0.360	0.071
S3	653	1.899	0.497	0.052
O3	675	1.837	0.547	0.047

The optical band gap energy of each silver-cadmium chalcogenide/polyamide composite shows the red shift as compared with that of corresponding starting material and matches the visible region of the solar spectrum. Many factors can contribute to the $E_{op.g}$ of such complex silver-cadmium chalcogenide/polyamide hybrid material like complex overall conduction and valence band alligment mechanism, a lot of various defects in band gap and changes either with particles size or strain [47–48].

3.3.2 Urbach energy

As seen in Figs. 3–5 absorption increases exponentially with the photon energy near the fundamental absorption edge. This region is known as the Urbach tail. A number of tail originating mechanisms including the presence of point defects and extended states at the valence or conduction bands; disordered structure; excitonic transitions or the presence of inhomogeneous strain in the semiconductor were discussed in scholar literature [49–50]. Urbach enegry is a measure of disorder in the semiconductor material and is related with the absorption coefficient by the following exponential equation [51]:

$$\alpha = \alpha_0 e^{h\nu/E_U} \tag{3}$$

where α_0 – constant, E_U – Urbach energy (eV) and $h\nu$ – photon energy (eV).

Urbach energy (E_U) for each composite was calculated using the slope determined from the linear portion of the plot between ln(A) versus 1/λ (Figs. 9−11) according to the following realation:

$$E_U \cdot tg\alpha = 1239.83 \tag{4}$$

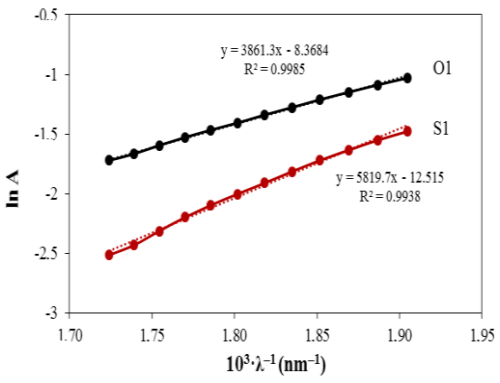

Fig. 9. Urbach plots for silver-cadmium chalcogenide/polyamide O1 and starting S1 composites.

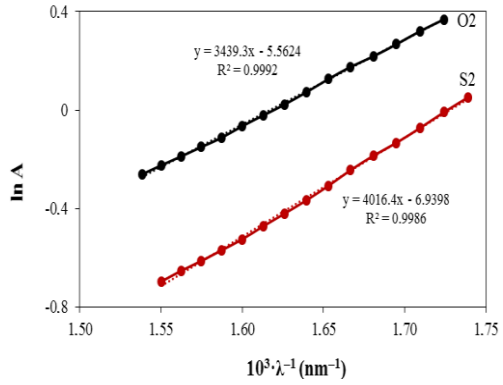

Fig. 10. Urbach plots for silver-cadmium chalcogenide/polyamide O2 and starting S2 composites.

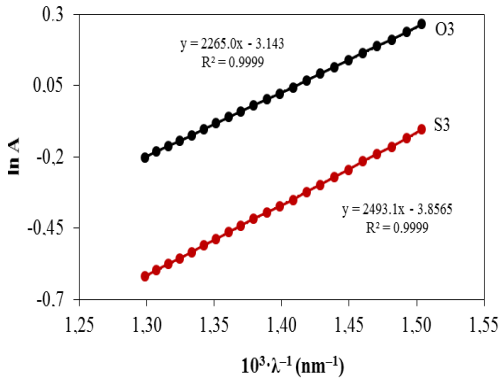

Fig. 11. Urbach plots for silver-cadmium chalcogenide/polyamide O3 and starting S3 composites.

Urbach energies for all studied hybrid materials are inserted in Table 3.

The Urbach energy of starting materials is in the range of 0.213–0.497 eV, which is relatively lower as compared with other organic-inorganic hybrid materials [52]. Relatively high Urbach energy indicates great tendency to convert weak structural bonds into defects [53]. In starting material these defects can originate from different structural bonds between the PA 6 amide (NH–CO) groups and the inorganic constituents, namely $SeS_2O_6^{2-}$, $SeSO_3^{2-}$, $Se_2S_2O_6^{2-}$ anions [23]. The presence of the amorphous selenium and polycrystalline CdS and CdSe in polymer host also significantly contributes to defects concentration.

As the Table 3 shows, there is a largest increase of Urbach energy in case of O1 composite as compared with coresponding starting S1 material. The increase in Urbach energy indicates the formation of more disordered structure, defects and the expansion of localized states into the band gap region with Cd^{2+} substitution by Ag^{+} ions. The increase of Urbach energy can also be related with the light scattering by the heterogeneous surface of the silver-cadmium chalcogenide/polyamide composites. The red shift of optical band gap correlates with the increase of Urbach energy implying that the transitions across the band gap and the transitions responsible for the Urbach tail are the electronic transitions.

The steepness parameter σ characterizes the broadening of the optical absorption edge arising from the electron-phonon or exciton-phonon interactions [54]. The steepness parameter is realeted with Urbach energy the by following equation:

$$\sigma = \frac{k \cdot T}{E_U} \tag{5}$$

where k is the Boltzmann constant, $8.617343 \cdot 10^{-5}$ eV/K and T the absolute temperature assumed to be 298 K.

The calculated values of σ are listed in Table 3.The steepness parameter of silver–cadmium chalcogenide/polyamide composite is lower than that of starting material.

3.3.3. Refractive index and dielectric constants at the fundamental absorption edge

In general, refractive index is a measure of semiconductor transparency to the incident photon [53] and is essential for future materials application in optoelectronic devices. The refractive index (*n*) at the fundamental absorption edge was calculated using the value of optical band gap energy via various empirical formulas proposed in reacently published papers [55–56]:

$$\text{Dimitrov and Sakka:} \quad \frac{n^2-1}{n^2+2} = 1 - \left(\frac{E_{op.g}}{20}\right)^{1/2} \tag{6}$$

$$\text{Tripathy: } n = n_o \cdot \left[1 + \alpha \cdot e^{-\beta \cdot E_{op.g}}\right], \tag{7}$$

where n_o = 1.73, α = 1.9017 and β = 0.539 eV^{-1} are the constant parameters, respectively.

$$\text{Ravindra relation: } n = 4.084 - 0.62E_{op.g} \tag{8}$$

$$\text{Herve–Vandamme relation: } n^2 = 1 + \left(\frac{A}{E_{op.g}+B}\right)^2, \tag{9}$$

where A is the hydrogen ionization energy 13.6 eV and B = 3.47 eV is a constant assumed to be the difference between the UV resonance energy and band gap energy.

The refractive index (*n*) estimated via various empirical formulas for silver-cadmium chalcogenide/polyamide as well as starting composites is listed in the Table 4.

Table 4. Refractive index (n), optical static dielectric constant (ε_0) and optical high frequency dielectric constant (ε_∞) values of studied composites.

Composite	ε_0	Dimitrov and Sakka		Tripathy		Ravindra		Herve–Vandamme	
		n	ε_∞	*n*	ε_∞	*n*	ε_∞	*n*	ε_∞
S1	7.528	2.554	6.523	2.597	6.744	2.549	6.499	2.498	6.242
O1	7.059	2.642	6.980	2.717	7.382	2.699	7.284	2.586	6.687
S2	7.369	2.694	7.259	2.794	7.806	2.785	7.760	2.640	6.975
O2	7.634	2.727	7.434	2.834	8.032	2.829	8.007	2.670	7.129
S3	8.202	2.782	7.740	2.912	8.479	2.907	8.448	2.723	7.414
O3	8.512	2.810	7.980	2.952	8.714	2.945	8.673	2.750	7.563

The silver-cadmium chalcogenide/polyamide composites are optically denser as compared to the corresponding starting samples. The heterogeneous large surface area also significantly contributes to higher light scattering ability.

The dielectric behavior of composite materials is important for its application in electronic devices. The high frequency dielectric constant (ε_∞) of composites was calculated from the following relation [57]:

$$\varepsilon_\infty = n^2 \tag{10}$$

The optical static dielectric constant (ε_0) of composites was calculated from the following relation [57]:

$$\varepsilon_0 = -33.26976 + 78.61505 \cdot E_{op.g} - 45.70795 \cdot E_{op.g}^2 + 8.32449 \cdot E_{op.g}^3 \quad (11)$$

The calculated values of static and high frequency dielectric constants are presented in Table 4. Static dielectric constants of silver-cadmium chalcogenide/polyamide composites as compared to those of starting composites increase, which indicate that polarization ability also increases. The values of optical static dielectric constants are higher than 7, which in turn suggests high-dielectric constant materials.

4 Conclusions

The morphological and optical properties of silver-cadmium chalcogenide/polyamide composites obtained by cation-cation exchange reaction using organic–inorganic hybrid cadmium chalcogenide/polyamide composite as a starting material have been investigated. The following conclusions can be drawn on the grounds of the obtained results and their interpretation:

After the cation exchange with Ag^+ in the aqueous solution, the surface morphology of the starting material transfers to a complex architecture demonstrating the intrinsic property of the cation exchanger. Silver-cadmium chalcogenide/polyamide composites exhibit heterogeneous surface morphology composed of agglomerates, voids, etc.

The silver-cadmium chalcogenide/polyamide composites absorption spectra are a superposition of the individual absorption spectra of different band gap materials within polyamide 6 network. The values of direct optical band gap energy ($E_{op.g}$) are within the range of 2.731–1.984 eV. The Urbach energy is in the range of 0.321–0.547 eV, which testifies to the high density of the localized tail states.

The refractive index, static and high frequency dielectric constants of silver-cadmium chalcogenide/polyamide composites were found to increase compared to those of starting composites.

Finally, the silver-cadmium chalcogenide/polyamide composites with optical band gaps in the visible spectral range, high refractive indices appear promising candidates for future anti-reflection coatings and in optoelectronic components.

References

[1] N. Gupta, G. F. Alapatt, R. Podila, R. Singh, K.F. Poole, Int. J. Photoenergy, 2009.
[2] B. Gates, B. Mayers, Y. Wu, Y. Sun, B. Cattle, P. Yang, Y. Xia, Adv. Funct. Mater. **12**(10), 679 (2002).
[3] H. J. Kong, S. Kim, T.-H. Le, Y. Kim, G. Park, C. S. Park, O. S. Kwon, H. Yoon, Nanoscale **9**(44), 17450 (2017).
[4] J. Jang, H. Yoon, Adv. Mater. **15**(24), 2088 (2003).
[5] P. A. Savarimuthu, Mater. Lett. **63**(9-10), 773 (2008).
[6] I.-S. Bae, S.-J. Cho, W.-S. Choi, B.-Y. Hong, Y.-J. Kim, Y.-M. Kim, J.-H. Boo, Thin Solid Films **516**(11**)**, 3577 (2007).
[7] A. Sahu, B. Russ, N. C. Su, J. D. Forster, P. Zhou, E. S. Cho, P. Ercius, N. E. Coates, R. A. Segalman J. J. Urban, J. Mater. Chem. A **5**(7), 3346 (2017).
[8] X. Jiang F., Chen W. Qiu, Q.Yan, Y. Nan, H. Xu, L.Yang, H. Chen, Sol. Energy Mater. Sol. Cells **94**(12), 2223 (2010).
[9] C. Borriello, A. Bruno, R. Diana, T. Di Luccio, P. Morvillo, R. Ricciardi, F. Villani, C. Minarini, Phys. status solidi A **212**(2), 245 (2015).
[10] V. Krylova, M. Andrulevicius, Int. J. Photoenergy, 2009.
[11] V. Krylova, J. Baltrusaitis, Appl. Surf. Sci. **282**, 552 (2013).

[12] V. Krylova, A. Milbrat, A. Embrechts, J. Baltrusaitis, Appl. Surf. Sci. **301**, 134 (2014).
[13] L. Chen, H. Gong, X. Zheng, M. Zhu, J. Zhang, S. Yang, B. Cao, Mater. Res. Bull. **48**(10), 4261 (2013).
[14] B. J. Beberwyck, Y. Surendranath, A. P. Alivisatos, J. Phys. Chem. C **117**(39), 19759 (2013).
[15] G. D. Moon, S. Ko, Y. Min, J. Zeng, Y. Xia, U. Jeong, Nano Today **6**, 186 (2011).
[16] X. Xu, X. Wang, Y. Zhang, P.Li, Solid State Sci. **61**, 195 (2016).
[17] W. Shi, J. Shi, S. Yu, P. Liu, Appl. Catal., B **138-139**, 184 (2013).
[18] V. Krylova, S. Žalenkienė, N. Dukstienė, J. Baltrusaitis, Appl. Surf. Sci. **351**, 203 (2015).
[19] M. Noh, T. Kim, H. Lee, C.K. Kim, S.W. Joo, K. Lee, Colloids Surf. A Physicochem. Eng. Asp. **359**(1-3), 39 (2010).
[20] R. Harpeness, O. Palchik,A. Gedanken, V. Palchik, S. Amiel, M. A. Slifkin, A. M. Weiss, Chem. Mater. **14**(5), 2094 (2002).
[21] R. Zamiri, H. A. Ahangar, A. Zakaria, G. Zamiri, M. Shabani, B. Singh, J. M. F. Ferreira, Chem. Cent. J. **9**(28), (2015).
[22] V. Krylova, N. Dukstienė, Appl. Surf. Sci. **470**, 462 (2019).
[23] V. Krylova, N. Dukstienė, S. Žalenkienė, J. Baltrusaitis, Appl. Surf. Sci. **392**, 634 (2017).
[24] M. E. Sánchez-Vergara, D. M. López-Romero, P. Vidal-García, C. Jiménez-Jarquín, A. Hernandez-García, O. Jiménez-Sandoval, Electron. Mater. Lett. **13**, 191 (2017**)**.
[25] S. Žalenkienė, V. Krylova, J. Baltrusaitis, Appl. Surf. Sci. **325**, 175 (2015).
[26] S. Feng, R. Xu, Acc. Chem. Res. **34**(3), 239 (2001).
[27] S. H. Mir, L. A. Nagahara, T. Thundat, P. Mokarian-Tabari, H. Furukawa, A. Khosla, J. Electrochem. Soc. **165**(8), B3137 (2018).
[28] Y. C. Li, H. Z. Zhong, R. Li, Y. Zhou, C. H. Yang, Y .F. Li, Adv. Funct. Mater. **16**, 1705 (2006).
[29] J. Liu, P. Raveendran, Z. Shervani, Y. Ikushima, Chem. Commun. **22**, 2582 (2004).
[30] S. I. Sadovnikov, Y. V. Kuznetsova, A. A. Rempel, Nano-Struct. Nano-Objects **7**, 81 (2016).
[31] H. Wang, L. Qi, Adv. Funct. Mater. **18**, 1249 (2008).
[32] D. W. Ayele, Egypt. J. Basic Appl. Sci. **3**(2), 149 (2016).
[33] B. Ramezanloo, M. Molaei, M. Karimipour, J. Lumin. **204**, 419 (2018).
[34] B. Wang, Zh. Liu, J. Han, T. Hong, J. Zhang, Y. Li, T. Cui, Electrochim. Acta **176**, 334 (2015).
[35] K. Surana, I. T. Salisu, R. M. Mehra, B. Bhattacharya, Opt. Mater. **82**, 135 (2018).
[36] X. Xu, X. Wang, Y. Zhang, P. Li, Solid State Sci. **61**, 195 (2016).
[37] T. Dia, B. Chenga, W. Hob, J. Yua, H. Tang, Appl. Surf. Sci. **470**, 196 (2019).
[38] S. Shen, L. Guo, X. Chen, F. Ren, S.S. Mao, Int. J. Hydrog. Energy **35**, 7110 (2010).
[39] S. S. Bubenov, S. G. Dorofeev, P. A. Kotin, K. O. Znamenkov, T. A. Kuznetsova, Mendeleev Commun. **24**(4), 250 (2014).
[40] K. Asadpour-Zeynali, F. Mollarasouli, Sens. Actuator B Chem. **237**, 387 (2016).
[41] S. Padmaja, S. Jayakumar, R. Balaji, C. Sudakar, M. Kumaravel, V. Rajendran, M. Rajkumar, A. V. Radhamani, Mater. Sci. Semicond. Process **16**, 1502 (2013).
[42] S. Yılmaza, A. Ünverdib, M. Tomakinc, İ. Polatd, E. Bacaksıze, Optik **185**, 256 (2019).
[43] S. K. Tripathi, R. Kaur, Jyoti, Opt. Commun. **352**, 55 (2015).
[44] X. Lu, L. Li, W. Zhang, C. Wang, Nanotechnology **16**(10), 2233 (2005).
[45] D. Souri, Z. E. Tahan, Appl. Phys. B: Lasers Opt. **119**, 273 (2015).
[46] U. Schubert, Macromol. Symp. **267**, 1 (2008).
[47] M. Z. Ansari, N. Khare, Sci. Semicond. Process **63**, 220 (2017).
[48] E. Purushotham, N. G. Krishna, Bull. Mater. Sci. **37**, 773 (2014).
[49] G. Landi, H. Ch. Neitzert, C. Barone, C. Mauro, F. Lang, S. Albrecht, B. Rech, S. Pagano, Adv. Sci. (Weinh) **4**(10), 1700183 (2017).
[50] A. Cremades, L. Görgens, O. Ambacher, M. Stutzmann, F. Scholz, Phys. Rev. B **61**(4), 2812 (2000).
[51] D. Souri, K. Shomalian, J. Non Cryst. Solids **355**, 1597 (2009).
[52] H. Chamroukhia, Z. B. Hamed, A. Telfah, M. Bassou, A. Zeinert, R. Hergenröder, H. Bouchriha, Opt. Mater. **84**, 703 (2018).
[53] S. Rani, S. Sanghi, A. Agarwal, V. P. Seth, Spectrochim. Acta A **74**(3), 673 (2009).

[54] H. Kabir, M. M. Rahman, K. M. Uddin, A.H. Bhuiyand, Appl. Surf. Sci. **423**, 983 (2017).
[55] S. K. Tripathy, Opt. Mater., **46**, 240 (2015).
[56] V. Dimitrov, S. Sakka, J. Appl. Phys. **79**, 1736 (1996).
[57] L. Hannachi, N. Bouarissa, Phys. B: Condensed Matter. **404**(20), 3650 (2009).